Cell, Vol. 118, 591–605, September 3, 2004, Copyright ©2004 by Cell Press

Endocytosis by Random Initiation and Stabilization of Clathrin-Coated Pits

Marcelo Ehrlich,[1] Werner Boll,[1] Antoine van Oijen,[2] Ramesh Hariharan,[3] Kartik Chandran,[4] Max L. Nibert,[4] and Tomas Kirchhausen[1,*]

[1]Department of Cell Biology
Harvard Medical School and
The CBR Institute for Biomedical Research
200 Longwood Avenue
Boston, Massachusetts 02115

[2]Department of Chemistry and Chemical Biology
Harvard University
Cambridge, Massachusetts 02138

[3]Department of Computer Science
Indian Institute of Science
Bangalore, 560012
India

[4]Department of Microbiology and Molecular Genetics
Harvard Medical School
200 Longwood Avenue
Boston, Massachusetts 02115

Summary

Clathrin-coated vesicles carry traffic from the plasma membrane to endosomes. We report here the real-time visualization of cargo sorting and endocytosis by clathrin-coated pits in living cells. We have detected the formation of coats by monitoring incorporation of fluorescently tagged clathrin or its adaptor AP-2; we have also followed clathrin-mediated uptake of transferrin and of single LDL or reovirus particles. The intensity of a cargo-loaded clathrin cluster grows steadily during its lifetime, and the time required to complete assembly is proportional to the size of the cargo particle. These results are consistent with a nucleation-growth mechanism and an approximately constant growth rate. There are no strongly preferred nucleation sites. A proportion of the nucleation events are weak and short lived. Cargo incorporation occurs primarily or exclusively in a newly formed coated pit. Our data lead to a model in which coated pits initiate randomly but collapse unless stabilized, perhaps by cargo capture.

Introduction

Clathrin-coated vesicles are the most prominent carriers of traffic between the plasma membrane and early endosomes. A local, clathrin-associated invagination of the plasma membrane, a coated pit, pinches off to form a membrane-derived coated vesicle. Cargo molecules, such as receptors that have specific targeting sequences in their cytoplasmic tails, are recruited to coated pits through interaction of their targeting signals with adaptor proteins (Bonifacino and Traub, 2003; Brodsky et al., 2001; Kirchhausen, 1999). The life cycle of a clathrin-coated vesicle, from coat assembly, cargo loading, and vesicle budding to coat disassembly and cargo delivery, involves a sequence of regulated events on a time scale of seconds to minutes (Kirchhausen, 2000). Many of the steps have been inferred from biochemical and cell-structural studies (Conner and Schmid, 2003), and some have recently been observed using live-cell imaging techniques (Gaidarov et al., 1999; Merrifield et al., 2002, 2004; Rappoport and Simon, 2003).

Clathrin assemblies were first seen in living cells using transient expression of EGFP-tagged clathrin light chains (Gaidarov et al., 1999). Some of these assemblies were stationary and long-lived; others appeared and disappeared on a time scale of about a minute. A more detailed analysis of the later stages in assembly of selected coated pits, using somewhat different visualization techniques, showed that budding of a coated vesicle could be detected by an abrupt movement of the fluorescent clathrin cluster, followed by loss of the clathrin signal after 15–30 s—an event interpreted as uncoating (Merrifield et al., 2002). A sudden burst of dynamin associated with the coated pit, detected using dynamin1-EGFP, preceded budding. A different group, using dynamin2-EGFP, reported similar results but found a more continuous increase in the dynamin signal (Rappoport and Simon, 2003).

Do these observations on selected coated pits represent the full range of clathrin-associated events? To answer this question, we have undertaken an unbiased analysis of clathrin dynamics at plasma membranes of cells stably expressing EGFP- or YFP-tagged clathrin light chain A to label clathrin, and EGFP-tagged σ2-adaptin to label the plasma-membrane clathrin adaptor AP-2. In addition to coated pits that grow, bud, and uncoat as previously described, we detect a large number of relatively short-lived clathrin clusters, which may be abortive coated pits. By conjoining this analysis with studies of how single cargo molecules associate with individual clathrin-coated pits, we find that cargo is captured only by relatively "young" pits, which then continue to grow with a mean total lifetime now determined by the size of the cargo. These characteristics are consistent with the requirements of a system that must entrap cargo of highly variable size and shape.

Results

Expression of Fluorescently Labeled Clathrin and AP-2

We established a monkey BSC1 epithelial cell line stably expressing rat brain clathrin LCa-EGFP (Figure 1A), and we showed that this fusion protein labeled coated pits and vesicles and that it did not affect receptor-mediated endocytic traffic of transferrin (Figure 1B). In addition, we generated and characterized cell lines expressing LCa-YFP, which also colocalized with endogenous clathrin heavy chain and did not affect receptor-mediated endocytosis. At least 60% of the endogenous

*Correspondence: kirchhausen@crystal.harvard.edu

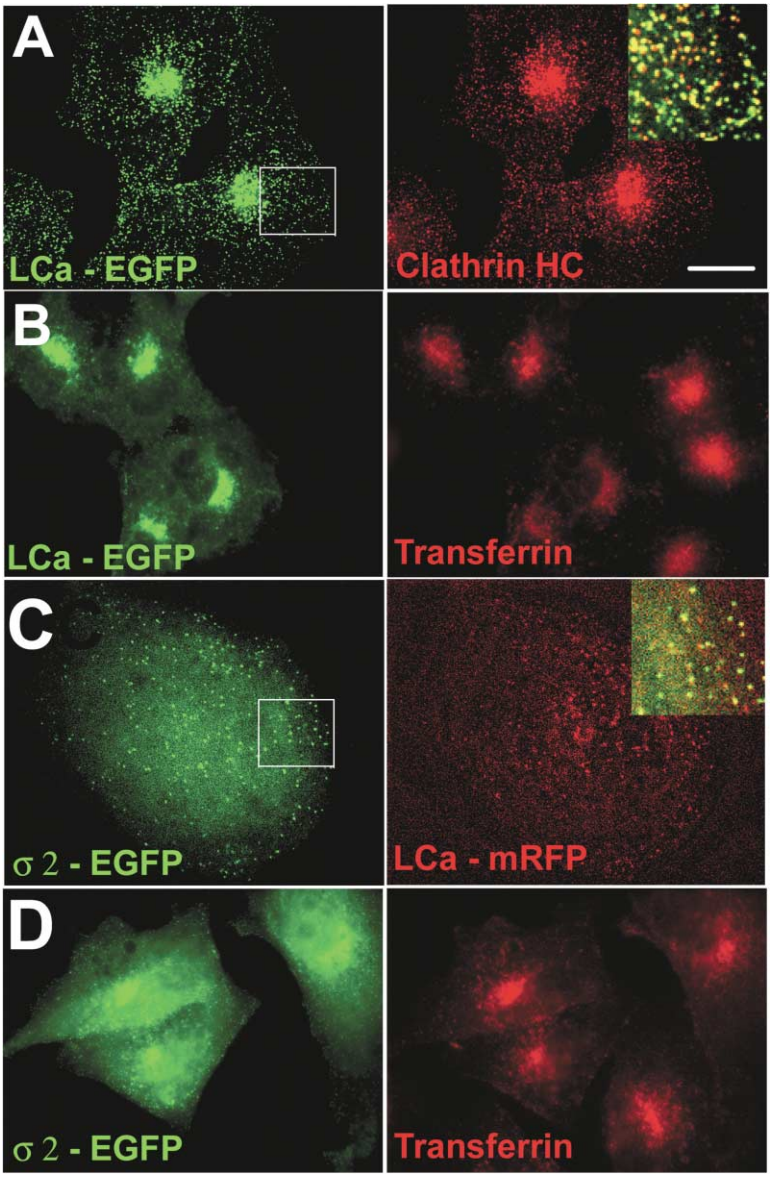

Figure 1. Labeling of Clathrin-Coated Structures with LCa-EGFP

(A) BSC1 cells stably expressing rat brain clathrin light chain LCa1 fused to EGFP (LCa-EGFP) (green) were fixed with 3.75% paraformaldehyde and labeled with the monoclonal antibody X22 specific for the heavy chain of clathrin (red). The epifluorescence views correspond to the bottom surface of the cell, in contact with the glass cover slip. The enlarged merged view of LCa-EGFP and endogenous clathrin heavy chain (upper right corner) corresponds to the section indicated by the square. The distribution of LCa-EGFP at the top and bottom cell surfaces displays the expected punctate pattern, and most clusters (92% ± 2%, 545 clusters in four cells) colocalize precisely with endogenous clathrin heavy chain. Scale bar, 10 μm.

(B–D) Expression of LCa-EGFP or σ2-EGFP had minimal effects on the uptake of transferrin and its traffic to endosomes. After the continuous uptake of 50 μg/ml transferrin labeled with Alexa647 (red) for 20 min at 37°C by a mixture of BSC1 cells stably expressing (or not) LCa-EGFP (green), the cells were fixed and imaged by epifluorescence microscopy. (D) BSC1 cells stably expressing σ2-EGFP (green) transiently expressing LCa-mRFP (red). The enlarged view corresponds to the bottom surface of the cell.

clathrin light chains LCa and LCb were replaced by LCa-EGFP or LCa-YFP, as determined by Western blot analysis of coated vesicles isolated from the expresser cells (data not shown). We also established a BSC1 cell line stably expressing the AP-2 rat brain σ2-adaptin fused at its C terminus to EGFP (Figure 1C). As expected, this fusion protein associated only with the plasma membrane and colocalized perfectly with transiently expressed clathrin LCa-mRFP (Figure 1C) and with endogenous AP-2 (data not shown). Its expression did not prevent uptake of transferrin (Figure 1D).

Dynamics of Clathrin and AP-2 Assemblies

We characterized the life cycle of the clathrin-coated pits and vesicles tagged with fluorescent clathrin and AP-2 using images acquired with a microscope configured with a confocal spinning disk (see Supplemental Movies S1–S4 at http://www.cell.com/cgi/content/full/118/5/591/DC1). The samples were alternately illuminated at two wavelengths using a time-lapse series designed to acquire up to 300 consecutive images at intervals of 2.6–20 s and for periods of up to 20 min. No significant differences were observed in the analyses described below when performed with images obtained by focusing on the top surface of the cell facing the medium, or with images obtained from the bottom surface, in contact with the supporting glass cover slip.

To track clathrin and AP-2 clusters along the time series automatically, all images were spatially filtered and segmented using SlideBook 4 (Experimental Procedures). The procedure successfully identified all clusters, as verified by visual inspection in randomly chosen images along the time series (Figure 2A and Supplemental Movies S3 and S4 on the *Cell* web site). The fluorescent clusters appeared as objects of 200–400 nm diameter, as expected for a coated pit or vesicle 100–200 nm in diameter, given the diffraction limit imposed by the transfer function of the microscope.

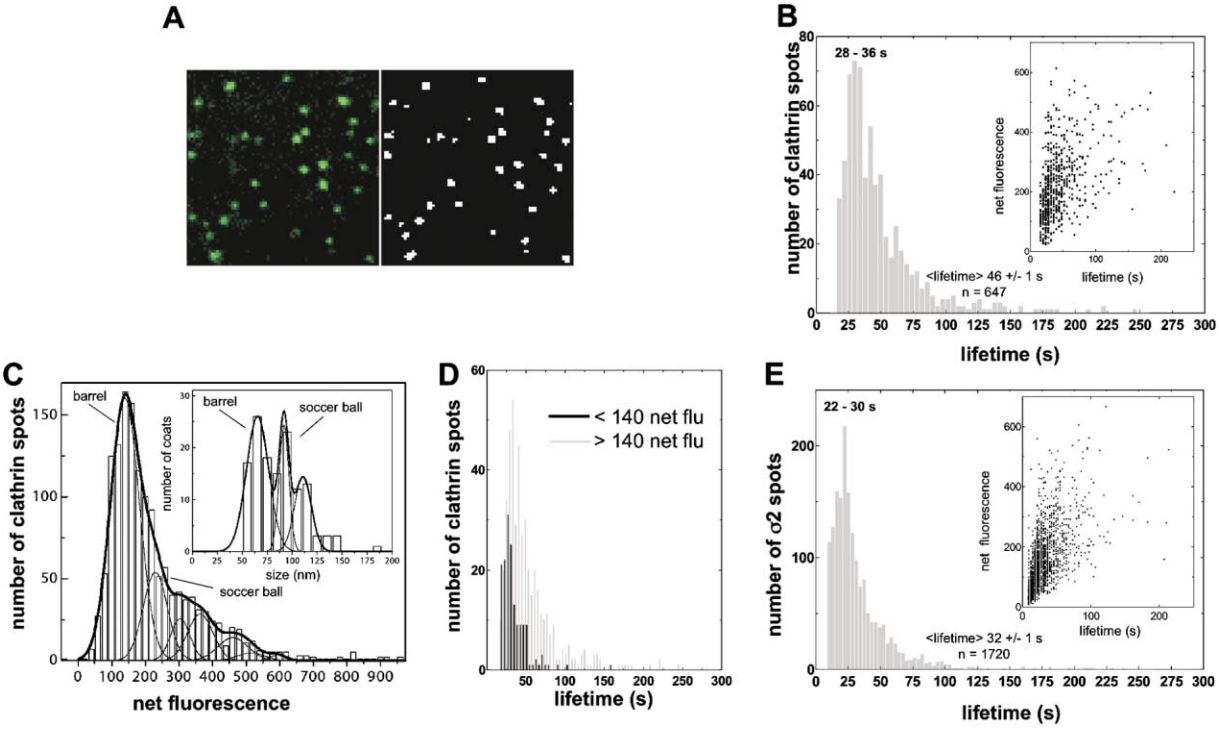

Figure 2. Dynamics of Clathrin Coats

(A) Validity check for automatic spot assignment in BSC1 cells expressing LCA-YFP. (Left panel) A representative raw image from a single time point acquired from the bottom surface of a BSC1 cell constitutively expressing clathrin LCa-YFP (green). The bright spots correspond to LCa-YFP clusters. (Right panel) Positions and shapes of the masks corresponding to the objects identified automatically by the spot recognition algorithm. The correctness of the particle-tracking procedure that follows the identity of single clathrin clusters during the time series was confirmed by visual inspection (see Supplemental Movie S3).

(B) Lifetime distribution for clathrin clusters in cells stably expressing LCA-EGFP. The distribution was determined from the elapsed time between the appearance and disappearance of every LCa-EGFP cluster present in the time series. Data were acquired from top and bottom surfaces of three different cells; only events appearing after the second time frame and disappearing before the last frame and lasting at least 16 s (four frames) are included. The inset shows the maximum net fluorescence intensity of each clathrin cluster (usually observed at the end of its life) as a function of its lifetime. The series was acquired every 4 s for a period of 7 min. Approximately 90 by 90 pixels (130 nm/pixel) were analyzed.

(C) Fluorescence intensity calibration. The distribution of net fluorescence intensities (fluorescence intensity for a given spot minus the fluorescence intensity of the background for an area of the same size) was determined for the diffraction-limited clusters present in a sample of chemically crosslinked coated vesicles purified from BSC1 cells expressing LCa-EGFP. The average net fluorescence intensity (140 and 230) and the relative contribution (55% and 17%) of the first two peaks were obtained from a multiple Gaussian fit. The inset shows the size distribution for an aliquot of the same sample, negatively stained with 1.2% uranyl acetate and imaged by electron microscopy. The relative contribution of the barrel (65–70 nm) and soccer ball (90–100 nm) coats is 55% and 22%, also from a multiple Gaussian fit.

(D) Lifetime distribution for the clathrin LCa-EGFP clusters shown in (B) separated according to their net fluorescence intensity into two groups of 482 and 165 spots with maximum net fluorescence intensity above and below 140, respectively.

(E) Distribution of lifetimes for AP-2 clusters in cells stably expressing σ2-EGFP. The distribution was determined from the elapsed time between the appearance and disappearance of every σ2-EGFP cluster present in the time series. Only events appearing after the second time frame and disappearing before the last frame and lasting at least 12 s (four frames) are included. The number of AP complexes in a coated pit is less than the number of LCa light chains (Kirchhausen, 1999), so that the σ2-EGFP signal for a given sized coated pit is weaker. The earliest time at which the AP complex can be detected is therefore slightly later than the earliest clathrin detection time. At current data collection rates, the difference is relatively minor. The inset shows the maximum net fluorescence intensity of each AP-2 cluster (usually observed at the end of its life) as a function of its lifetime. The series was acquired every 3 s for a period of 10 min. Approximately 90 by 90 pixels (130 nm/pixel) were analyzed.

The clathrin clusters appeared and disappeared with a mean lifetime of 46 s (Figure 2B). The most frequent events had a duration of 28–32 s and a net fluorescence intensity of 230. We used coated vesicles isolated from this cell line to relate the net fluorescence intensity values to the size of the coated pits (Experimental Procedures). The average intensity of these 28–32 s clusters just prior to disappearance (Figure 2B, inset) agreed very well with the fluorescence emitted by isolated coated vesicles 90–100 nm in diameter and therefore containing 60 triskelions (soccer ball design) (Figure 2C). The fluorescence intensities from longer-lived clathrin clusters corresponded to the signal from larger isolated coated vesicles with diameters between 100 and 200 nm. Thus, longer-lived clusters correspond to larger coated pits. The fluorescence intensity from a particular cluster increased as a function of time until the moment of its disappearance. We seldom found inactive fluorescent patches at the plasma membrane, and we did not observe diffraction-limited small spots emanating from

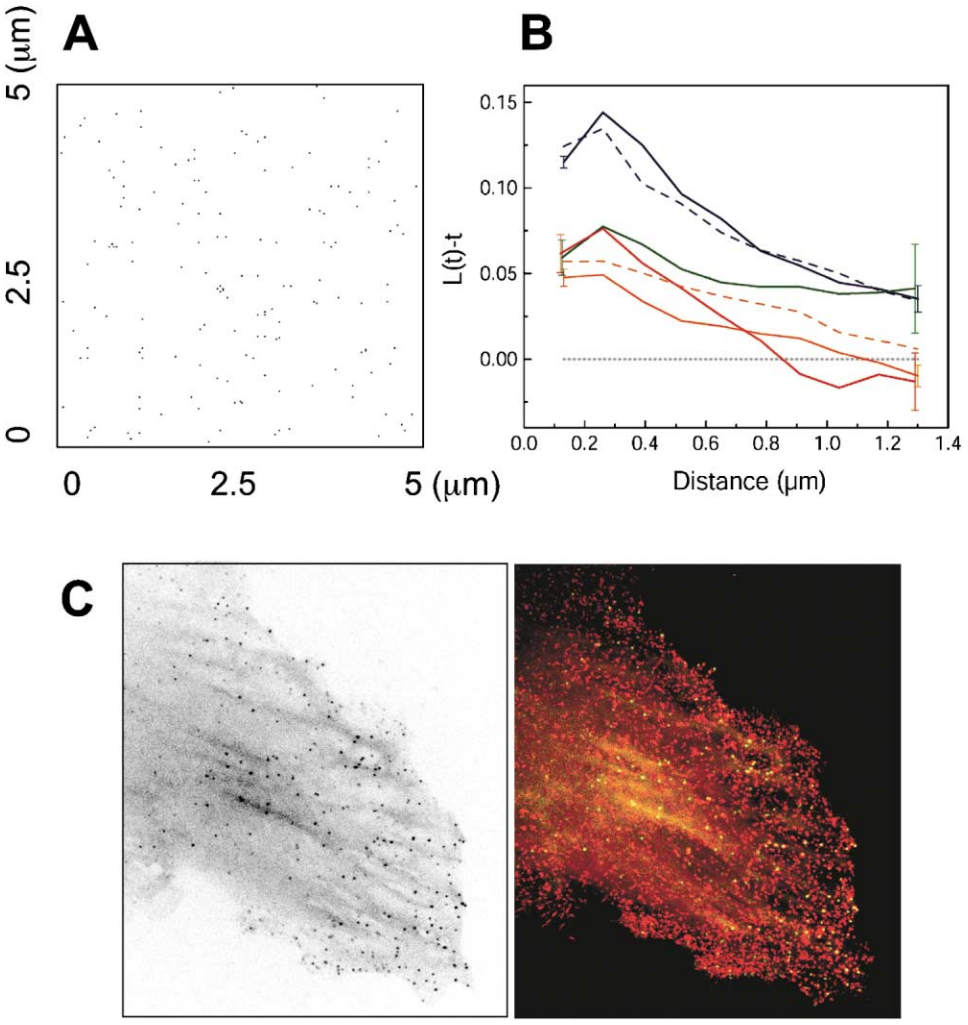

Figure 3. Sites of Formation of Clathrin-Coated Pits

(A) The 2D plot shows the locations in an imaged area at which new clathrin clusters appeared during the course of the 7 min time series analyzed in Figure 2B.

(B) Clustering analysis of the nucleation sites used by newly formed coated pits using Ripley's K function (Ripley, 1976). The solid lines are plots of the K function calculated from the experimental data of BSC1 cells expressing LCa-EGFP (orange and red) and σ2-EGFP (green) or from COS cells expressing LCa-EGFP (blue) and acquired every 2, 4, 3, or 4 s, respectively. The stippled lines correspond to simulated K functions with (gray) or without (orange and blue) Poissonian contributions to rationalize the observed deviations from Poissonian behavior. The orange dotted line is obtained from a distribution of events in a field of active patches 400 nm in diameter surrounded by inactive rims of 200 nm wide. The blue line is obtained by combining this geometry with nonactive, empty regions (inactivation of 50% of the field by multiple empty regions, each having a diameter varying from 500 nm to 2.6 μm). Both simulated curves are obtained with datasets that have a number of events and observation area similar to those in the experimental data sets.

(C) Location of AP-2 clusters in the first time frame (left panel, black; right panel, yellow) compared to the location of all the AP-2 clusters projected as a single frame (right panel, red) from the BSC1 stably expressing σ2-EGFP used for (B) and Supplemental Movie S2. These images illustrate the absence of preferred sites for coat assembly.

stable clusters, in contrast to some previous observations (Gaidarov et al., 1999; Rappoport and Simon, 2003). We did see stable clusters that persisted for at least 200 s on the bottom surface of COS cells transiently expressing LCa-EGFP or LCa-YFP. We believe that these stable clusters are the large, flat clathrin arrays seen by electron microscopy on the bottom surfaces of cells (Heuser, 1989). The on-off dynamics of LCa-EGFP in BSC1 and COS cells were similar (data not shown). We saw no stable patches of σ2-EGFP in the BSC1 cells; all the σ2-EGFP clusters showed the on-off behavior just described for clathrin (Figure 2E).

A number of clusters (~25% of total) had low intensity (net fluorescence intensity of 140 or less) and appeared and disappeared with lifetimes of 16–28 s (Figure 2D). These were identified and tracked by the software with a certainty of greater than 99.95% (Supplemental Data), and their assignments were verified manually. Their intensity corresponds to no more than 30 triskelions, indicting that, whatever these events represent, they cannot be complete coated vesicles. They may represent abortive coated pits (see below). The remaining clusters, of greater intensity, displayed a broader distribution of lifetimes, peaking between 28 and 36 s. The lifetime

distribution for σ2-EGFP clusters resembled that for clathrin clusters but shifted toward shorter times by about 6 s (Figure 2E).

The rate of appearance of new clathrin clusters lasting at least 20 s was about three events per 10^8 nm^2 s^{-1}. Assuming that the majority of these events correspond to a 100 nm diameter coat, this rate can readily account for the observed capacity of cell in culture to internalize about 1%–2% of cell membrane in 1 min through the clathrin pathway (Hansen et al., 1992). As expected, the dynamic on-off behavior of all of these clathrin clusters was prevented by conditions known to interfere directly or indirectly with clathrin coat assembly (Supplemental Movies S5–S7). It is therefore likely that most of the on-off events of lifetime equal to or greater than 24–28 s include all steps of clathrin coat assembly: nucleation of a coated pit, completion of growth, transformation into a coated vesicle by budding, and vesicle uncoating.

Initiation Sites

The majority of clathrin (or σ2) clusters in BSC1 cells appeared on the cell surface at sites that were not reused during the observation time (Figures 3A and 3C). Because the cells were stationary during the acquisition time, we can rule out the trivial explanation that global motion is responsible for the low frequency of spatial colocalization of nucleation sites. We performed a clustering analysis based on use of a scaled form of Ripley's K function (Ripley, 1976) (Supplemental Data). The results, presented in Figure 3B, compare data sets (solid lines) acquired from BSC1 cells, stably expressing LCa-EGFP or σ2-EGFP, with simulations of distributions with identical field and sample size as the experimental data (ten simulations per dataset, dashed lines). The K function analyses for data from BSC1 cells show clearly detectable non-Poissonian components. To simulate compartmentalization of the plasma membrane into domains of free diffusion bounded by diffusion barriers (generally ascribed to cytoskeletal elements), we performed the analysis using a model in which an active field of random nucleation is surrounded by an inactive rim. The dimensions that best fit the observed distribution are 400 nm for the diameter of the active patches and 200 nm for the width of the inactive rim. These dimensions are roughly consistent with compartments in the plasma membrane of 230–750 nm in diameter displaying free Brownian movement of single phospholipids or transferrin and α 2-macroglobulin receptor molecules (Fujiwara et al., 2002; Sako and Kusumi, 1994). We conclude that the nonrandom contribution to the spatial distribution of nucleation sites can best be described by a restriction to active regions but not by localized, specialized structures.

We also analyzed data from COS cells transiently expressing LCa-EGFP, for which coincidences of nucleation sites during the observation time were much more frequent. Indeed, from studies with COS cells, Gaidarov et al. (1999) postulated that there are "hot spots"—privileged sites for coated-pit nucleation. We could model our COS cell data by introducing large regions of inactive membrane into the model for active patches described above. The best fit to the data analyzed in Figure 3B was obtained by assuming that about 50% of the cell surface was inactive for coated pit formation and that these inactive regions varied in diameter from 0.5 to 2.6 μm. The inactive regions might correspond to folds in the cell surface, constraints imposed by the underlying cytoskeleton, or other special features of COS cells. We were unable to get a good fit by assuming restricted "hot spots" —that is, by using a small diameter for the active zone and a larger width for the inactive rim.

Correlated Dynamics of Clathrin, AP-2, and Dynamin in Coated Pits

We monitored the behavior of transiently expressed clathrin LCa-mRFP in BSC1 cells stably expressing σ2-EGFP. Every fluorescent spot containing σ2-EGFP colocalized with LCa-mRFP (Figure 1C) in living cells, and most (91%) colocalized with clathrin heavy chain in fixed cells (data not shown). The clusters found in the coexpressing cells displayed the same on-off behavior as those in cells expressing only tagged LCa or σ2, indicating that coexpression did not affect the assembly of coated pits and vesicles. For all spots, regardless of their age, the fluorescent signals for LCa and σ2 always appeared and disappeared together and with similar rates during the life of a cluster (Figure 4A). We conclude that clathrin and adaptor complexes coassociate in coated pits and that clathrin uncoating and adaptor dissociation also occur together.

Dynamin is required for budding of coated-vesicle membranes. We transiently expressed clathrin LCa-mRFP and dynamin2-EGFP in COS cells (Figures 4B–4E). The best time for imaging was 14 hr posttransfection, a time at which both proteins appear together in small, transient clusters (Supplemental Movie S8). Expression (particularly of dynamin) for longer intervals resulted in the appearance of numerous stationary clathrin and dynamin clusters, probably due to overexpression. We used the same filtering and segmentation procedure described above to identify clathrin and dynamin clusters in the transiently expressing COS cells. The clathrin clusters displayed the on-off behavior observed in BSC1 cells stably expressing LCa-EGFP or LCa-YFP and had similar mean lifetimes. Most of the clathrin clusters with lifetimes of 30 s or longer contained dynamin (Figures 4B and 4C). Many of the dynamin clusters did not contain clathrin, however; these probably represented caveolae or podosomes (Orth and McNiven, 2003). The colocalizing clathrin and dynamin signals both increased steadily during the lifetime of the cluster (Figures 4C–4E), and the strength of the dynamin signal often showed an acute increase, followed by a sharp decrease, prior to the disappearance of the associated clathrin signal (Figure 4E). By contrast, the short-lived clathrin clusters rarely exhibited this burst (Figure 4D), although the dynamin and clathrin signals still disappeared together (Supplemental Movie S8).

Real-Time Imaging of LDL Endocytosis

Are the dynamics of clathrin analyzed in this way representative of coated pits that actually entrap and take up single cargo molecules? We briefly (0–15 min) incubated BSC1 cells expressing LCa-YFP with 0.72 μg/ml LDL labeled by fluorescent DiI (DiI-LDL) or BSC1 cells expressing LCa-EGFP with LDL labeled by Alexa594 (Reyn-

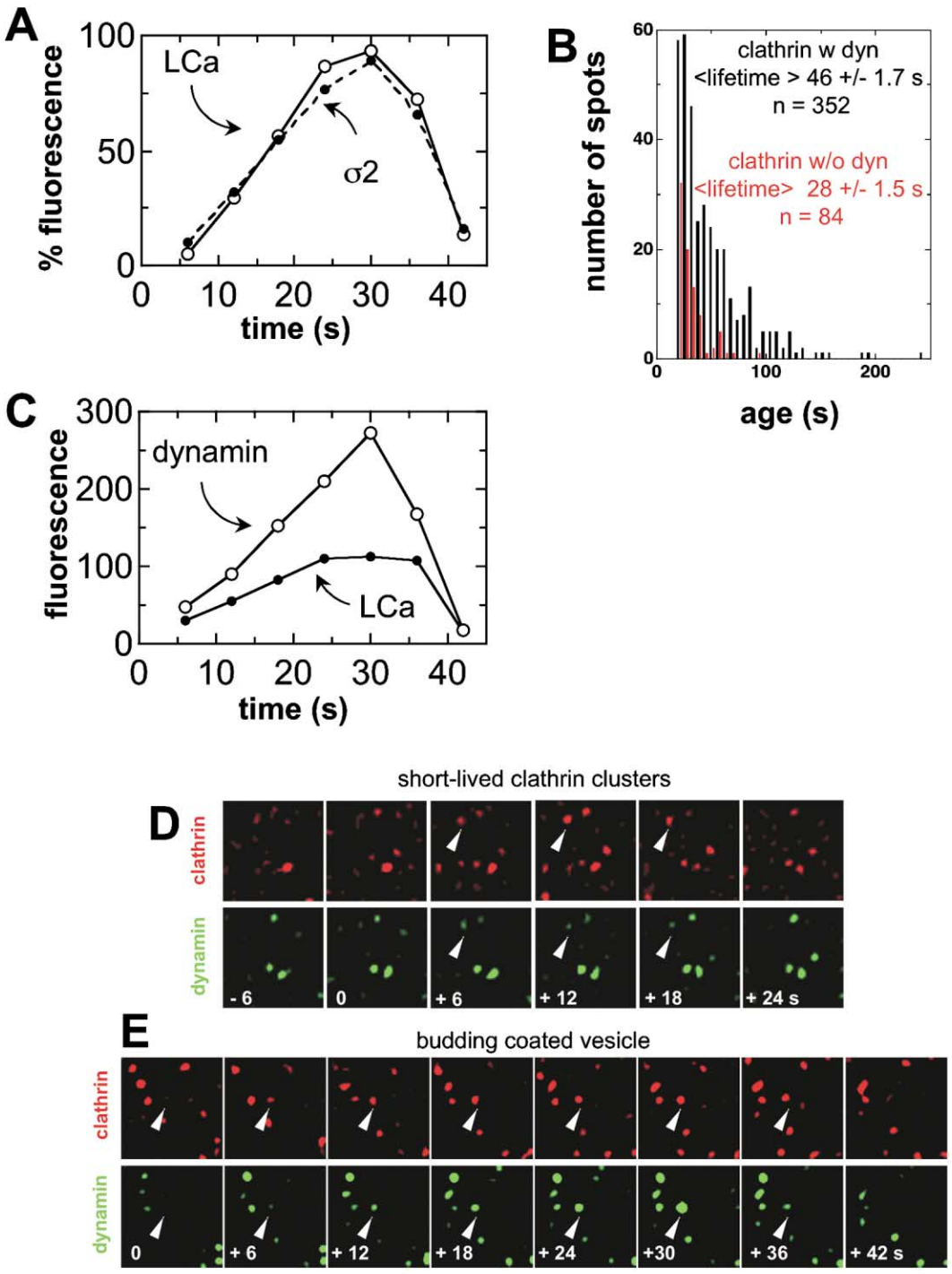

Figure 4. Dynamics of Clathrin, AP-2, and Dynamin in Coated Pits

(A) Plot of the fluorescence normalized to the highest value before uncoating of 28 coated pits containing σ2-EGFP and LCa-mRFP, each with a lifetime of 42 s. The data were obtained from three BSC1 cells stably expressing σ2-EGFP and transiently expressing LCa-mRFP.

(B) Comparison of the distributions of clathrin lifetimes in clusters containing clathrin and dynamin and in those from which dynamin was absent (or below detection limit). The data were obtained from COS cells transiently expressing clathrin LCa-mRFP and dynamin2-EGFP, imaged with the spinning disk confocal 14 hr posttransfection every 6 s and for a period of 6.5 min and approximately 90 by 90 pixels (130 nm/pixel).

(C) Fluorescence intensity for dynamin2-EGFP and for LCa-mRFP determined for a subset of 22 clathrin clusters, each with a lifetime of 42 s.

(D and E) Expanded views of a short-lived clathrin cluster (abortive pit) and a budding coated vesicle. The time series were obtained from a COS cell expressing LCa-mRFP (red) and dynamin2-EGFP. Times are defined by the moment of appearance of the clathrin signal. The top (D) and bottom (E) panels represent examples of short- and long-lived clathrin clusters, respectively. While the fluorescence signals of clathrin and dynamin disappear synchronously in the short-lived abortive pit, the dynamin signal further increases in the budding coated vesicle just before both signals disappear.

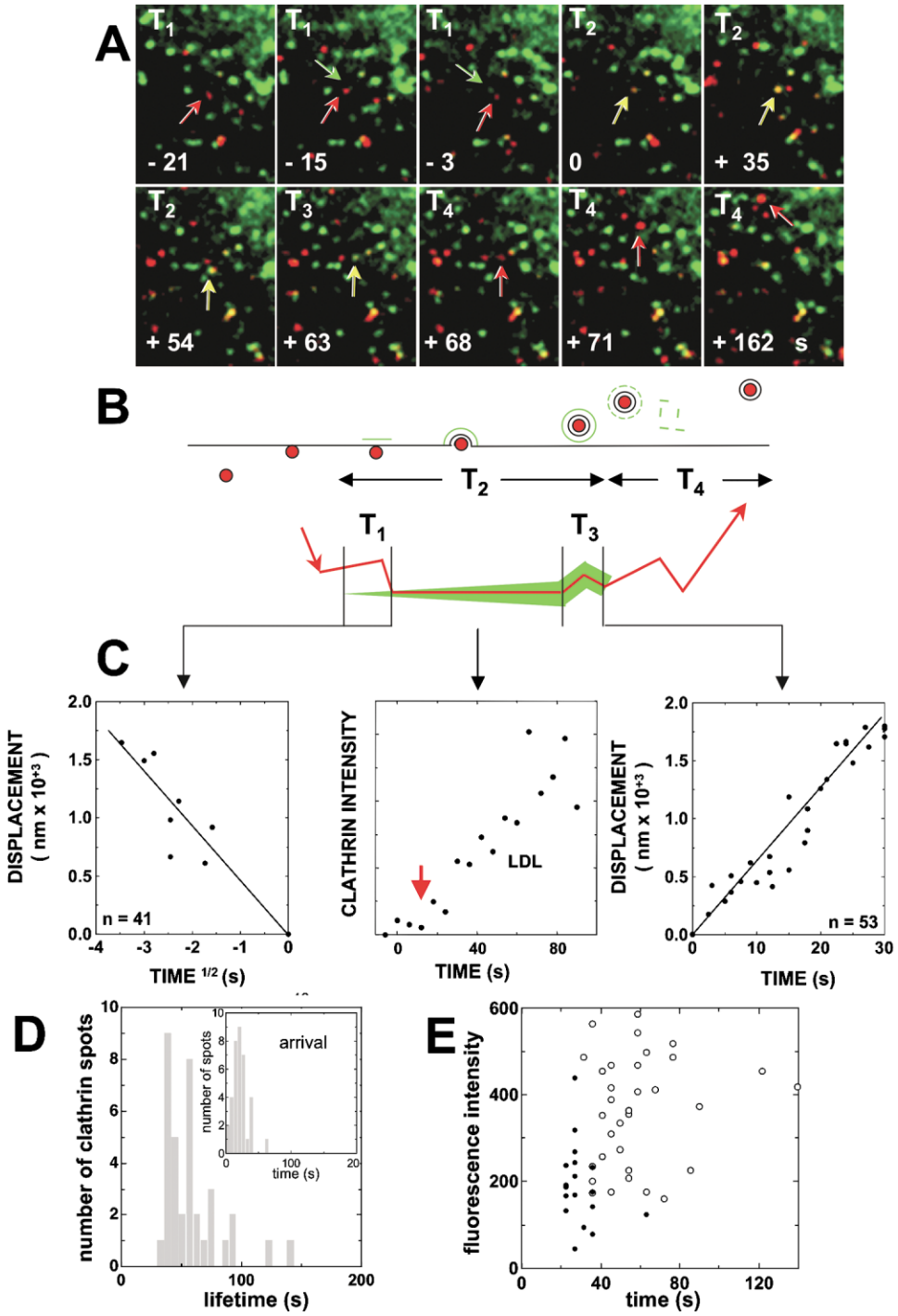

Figure 5. Dynamics of Capture and Internalization of Single DiI-LDL by Clathrin-Coated Pits and Vesicles

(A) Expanded views from a time series of DiI-LDL and LCa-YFP, imaged by fluorescence microscopy using the spinning disk confocal microscope. Times are defined from the moment of association of single DiI-LDL particles with clathrin clusters, as illustrated in the schematic drawing (B). T_1–T_4 represent the intervals before association (T_1), during association (T_2), joint lateral motion of LDL and clathrin prior to uncoating (T_3), and motion of LDL after uncoating (T_4), respectively. Average and standard errors are shown. (C) The left and right panels contain plots for the average displacement of DiI-LDL before its association with clathrin (T_1) and upon initiation of its lateral motion ($T_3 + T_4$) as a function of $t^{1/2}$ and t, respectively. The middle panel is a representative example showing the increase in the net fluorescence intensity for the LCa-YFP signal from a single clathrin pit during its association with one DiI-LDL particle. The red arrow indicates the time of encounter of DiI-LDL particle with a preformed and relatively dim clathrin pit. Note that $t = 0$ corresponds to the appearance of the clathrin signal, not to the encounter as in (A). (D) Distribution of lifetimes for the clathrin clusters that incorporate Alexa594-LDL. The inset indicates the time of arrival of an LDL particle at a nascent coated pit. (E) Fluorescence intensity of a clathrin-coated pit at the time of arrival of an LDL particle (black circles) and before uncoating (white circles).

olds and St. Clair, 1985) and then followed the dynamics of coated pit formation (Figure 5 and Supplemental Movie S9). The uniform intensity of the diffraction-limited LDL fluorescence signals suggests that they correspond to single LDL particles. We confirmed that the uptake of DiI-LDL was clathrin dependent (Supplemental Movie S5).

We followed the trajectories of 63 single DiI-LDL particles identified on six cells labeled in four independent experiments (Figures 5A–5C). We selected particles that associated with clathrin clusters, which only happened on the top surface of the cell. Using SlideBook 4, we determined manually the centers of selected particles in the DiI-fluorescence channel and then again in the clathrin fluorescence channel. In this way, we found the position of a DiI-LDL molecule and the corresponding clathrin LCa-YFP cluster at each point during the time series. Prior to association with clathrin, most LDL particles moved diffusively on the membrane, as the distance traveled varied linearly with the square root of time (Figure 5C). The calculated diffusion coefficient was about 6×10^{-10} cm^2 s^{-1}, well within the range of reported values obtained by spectroscopic methods for the LDL receptor (Goldstein et al., 1981). The characteristics of this motion were similar to those exhibited by other LDL particles that did not associate with clathrin during the course of the time series. In most cases ($n = 41$), a DiI-LDL particle diffusing on the cell surface encountered a rather dim, relatively stationary clathrin-coated cluster (average age of 20 ± 2 s, with a typical fluctuation in lateral position of less than one to two pixels, or 100–200 nm). In a few cases ($n = 5$), the DiI particle appeared to land directly from the medium onto a young, preexisting clathrin cluster. In the remaining instances ($n = 17$), a migrating DiI-LDL particle stopped moving just as a clathrin cluster appeared beneath it. In all of these events, the fluorescence clearly continued to increase following association with the LDL particle (see example in Figure 5C). At the end of this period, the clathrin signal disappeared rapidly, presumably because of uncoating. Often, the clathrin-LDL objects executed an abrupt lateral displacement of 300–600 nm with an average speed of 57 nm s^{-1} for 11 ± 2 s just before disappearance of the clathrin signal. From observations using a combination of epifluorescence and TIRF, Merrifield et al. (2002) reported a similar lateral displacement (average speed of 44 nm s^{-1}) of LCa-dsRED in clathrin clusters, just before disappearance of the dsRED signal and immediately after appearance of a signal from dynamin1 fluorescently tagged with EGFP. Thus, the sudden displacement probably represents budding of the coated vesicle, for which dynamin is required, and release from the plasma membrane. The DiI-LDL particle then continued to move laterally after vesicle uncoating, and the distance traveled was linearly dependent on time, a characteristic of directed motion (Figure 5C). The position of the particles was hard to monitor beyond 30 s, because the particle disappeared from the field of observation due to a combination of axial and lateral motion.

Clathrin clusters active in LDL uptake, as identified by the association of Alexa594-LDL with LCa-EGFP, had mean lifetimes of 40 and 60 s (Figure 5D). Their mean net fluorescence intensity was 180 at the time of association with Alexa594-LDL, consistent with the capture of LDL particles by young pits (Figure 5E, black circles) and about 390 at the time of uncoating, corresponding to coats larger than 90–100 nm soccer balls (Figure 5E, clear circles).

Real-Time Imaging of Transferrin Endocytosis

To study recruitment of a much smaller cargo, we monitored the association of transferrin ($\sim$5 nm in diameter) with LCa-EGFP clusters in COS cells (Figure 6A). We exposed cells briefly (1 min) to transferrin labeled with Alexa568 (approximately three to four dyes per molecule) and followed the dynamics of capture and endocytosis by manual spot tracking. Within seconds of incubation, the plasma membrane became homogeneously labeled with Alexa568 transferrin and, soon thereafter, weak spots appeared. All these spots colocalized with growing clathrin clusters, suggesting that a transferrin receptor bound to its ligand can diffuse into a partially formed coat. Like LDL capture, incorporation occurred most frequently in newly formed coated pits (6–15 s post-appearance, Figure 6B, inset). Association of Alexa568 transferrin and LCa-EGFP lasted 24–50 s before uncoating (Figure 6B).

Real-Time Imaging of Reovirus Endocytosis

To examine coated pit dynamics during the uptake of a large cargo, we investigated the capture and endocytosis by clathrin-coated pits and vesicles of reovirus a nonenveloped, dsRNA virus that requires access to endosomes for successful infection (Figure 7 and Supplemental Movie S10). Its receptor is an Ig superfamily member known as JAM1 (Forrest et al., 2003); it also interacts with cell surface carbohydrates (Paul et al., 1989). An active clathrin endocytic pathway is important for successful infection (Supplemental Movies S11 and S12).

Upon landing on the upper surface of the cell (no virus could be detected bound to the bottom surface), Alexa647 reovirus particles were essentially stationary (average displacement of 5 ± 1 nm s^{-1} [$n = 17$] over periods of 280–1500 s). That is, the lateral mobility of the virus-receptor complex was substantially smaller than that of the LDL-LDL receptor. Eventually a clathrin signal appeared as a cluster colocalizing with the viral particle, and the two then remained associated with each other for 398 ± 49 s (Figure 7B), significantly longer than the 40–60 s association of clathrin with LDL (Figure 5D). Presumably, the longer association was due to the time required to build a larger clathrin lattice (the reovirus particle is about 85 nm in diameter; LDL is about 27 nm). Consistent with this interpretation, the intensity of the clathrin signal also increased during the full period in which clathrin and virus signals colocalized (Figure 7C).

At the end of the association period, we noticed (as with LDL) an abrupt disappearance of the clathrin signal and initiation of rapid lateral movement of the fluorescent virus particle. The virus particle acquired an average speed of 26 ± 0.2 nm s^{-1} (301 determinations for 34 viruses), and its path, which had the characteristics of directed rather than diffusive motion, could be followed for at least 120 s. We suggest that, as with LDL, the rapid, directed motion represents intracellular migration of the virus encased in a newly uncoated vesicle toward the appropriate endosomal compartment. Rapid and directed motion of reovirus was seen only after its

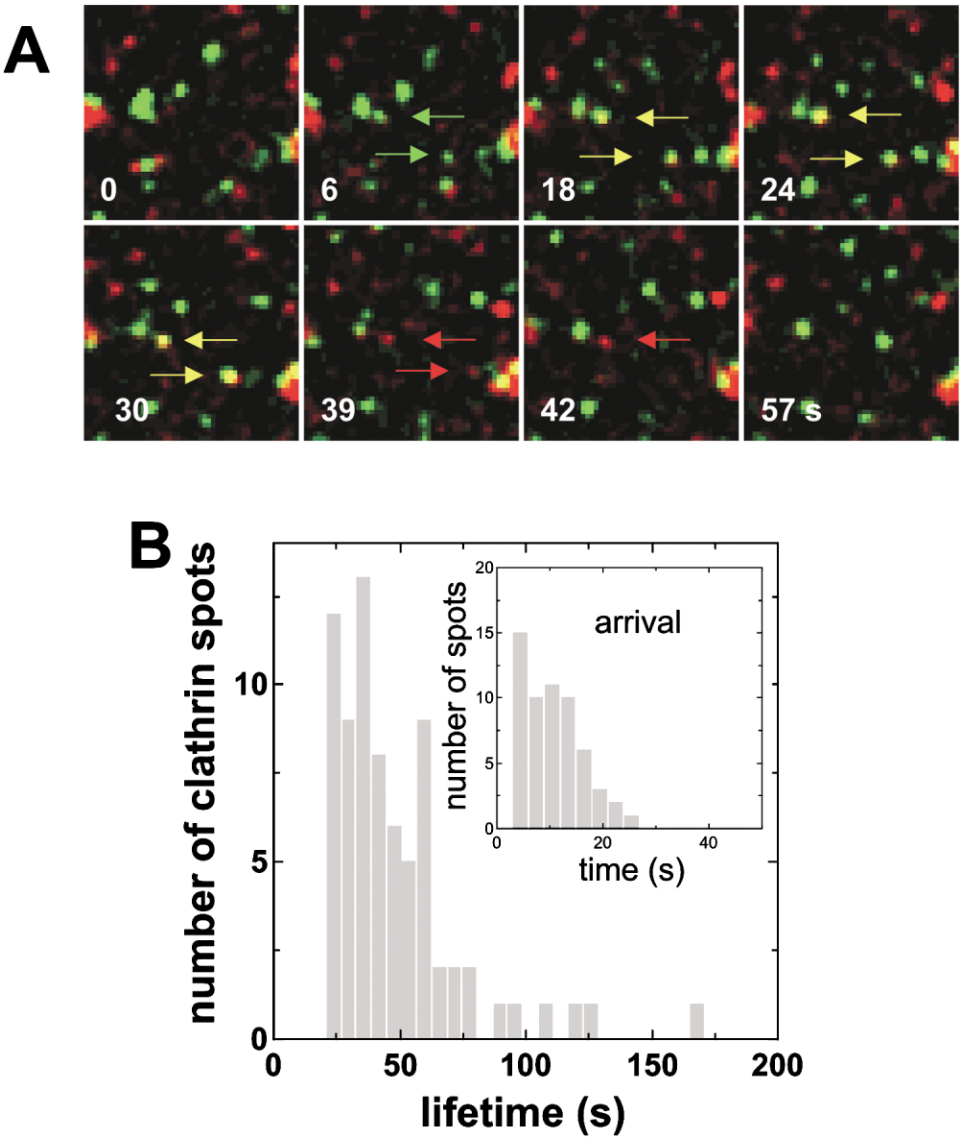

Figure 6. Dynamics of Capture and Internalization of Transferrin by Clathrin-Coated Pits and Vesicles

(A) Expanded views from a time series of Alexa568 transferrin and LCa-EGFP transiently expressed in COS cells, imaged by fluorescence microscopy using the spinning disk confocal microscope.

(B) Distribution of lifetimes for the clathrin clusters that incorporate Alexa568 transferrin. The inset indicates the time of arrival of transferrin at nascent coated pits.

association with clathrin (Figure 7A and Supplemental Movie S10) or, if this association was not detected, then only in areas that were clearly intracellular and after extensive exposure (over 1 hr) of the cells to the fluorescent virus (Supplemental Movie S12). Because rapid intracellular reovirus movement was seldom detected in cells not performing clathrin-mediated endocytosis (Supplemental Movies S11 and S12), we believe that the images showing colocalization of clathrin and reovirus represent a prominent cellular entry route for the virus.

Discussion

Clathrin Dynamics at the Plasma Membrane

The experimental analyses of clathrin coated pit formation presented here rely primarily on use of cell lines stably expressing EGFP- or YFP-tagged LCa or σ2-EGFP. We thus avoid artifacts associated with transient overexpression, and we can make consistent comparisons between population-based analyses of endocytic events and manual tracking of individual vesicles. In some cases, we briefly expressed fluorescently tagged LCa or dynamin to study the capture of transferrin or the association of AP-2 and dynamin with clathrin. We have recorded data from both top and bottom surfaces of the cells, and we have included in the statistics of coated-pit lifetimes all clathrin-containing clusters of diffraction limit size. Exclusion of larger clathrin clusters (and also weak and very mobile spots) eliminates highly mobile endosomes and also a small number of stationary clusters on the bottom surface that are probably large, flat arrays. The data presented here thus provide an objec-

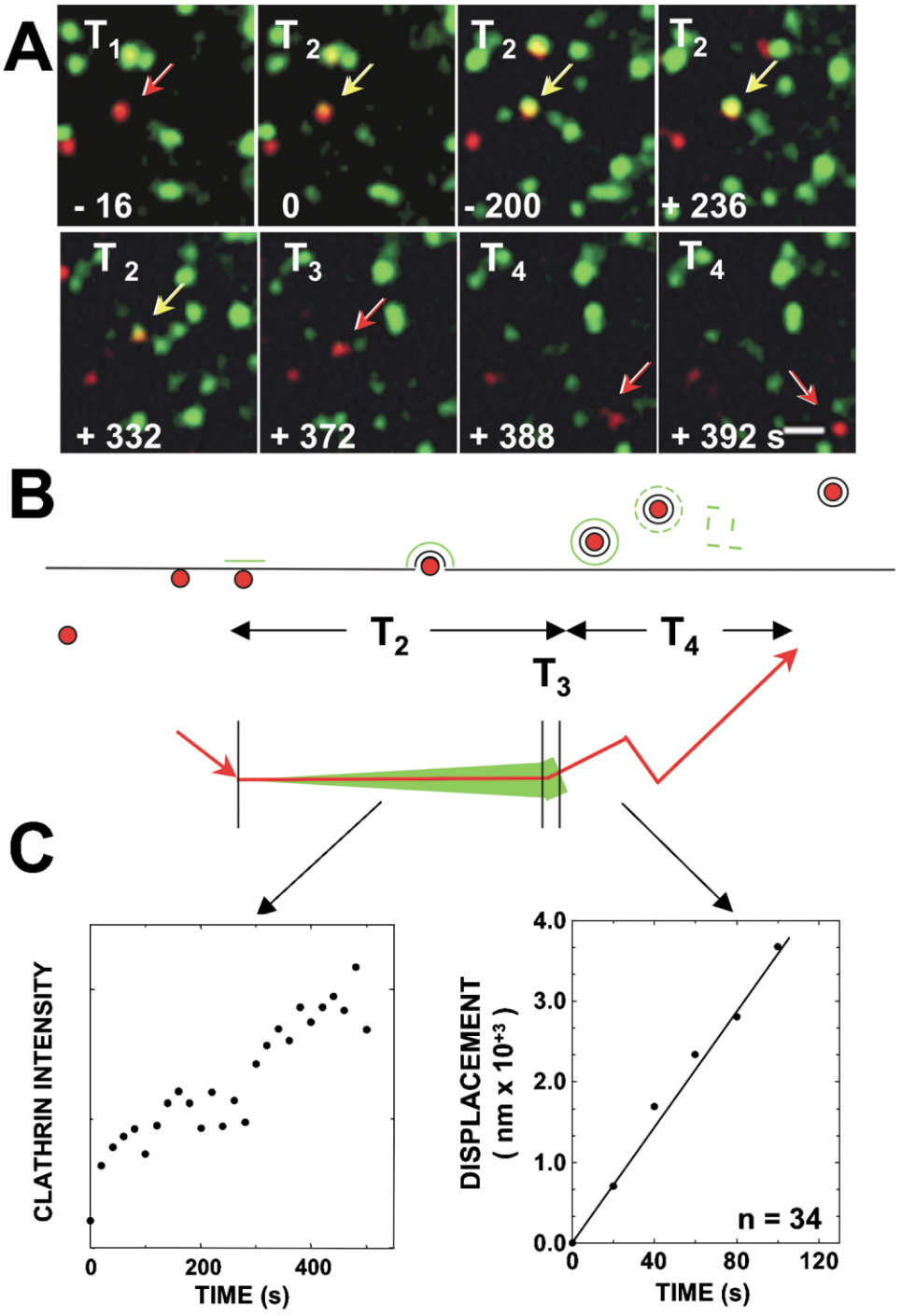

Figure 7. Dynamics of Capture and Internalization of Single Reovirus Particles by Clathrin-Coated Pits and Vesicles

(A) Expanded views of a time series of reovirus tagged with Alexa647 (red) and LCa-YFP (green) imaged as in Figure 5. Times are defined by the moment of association between reovirus and clathrin as illustrated in the schematic drawing (B). Average and standard errors are shown. (C) The panel on the left shows a representative example of the increase in the net fluorescence intensity of a clathrin pit during its association with a single reovirus particle. Differences in imaging conditions preclude a direct comparison of absolute fluorescence intensities with the data in Figure 5. The plot on the right shows the average displacement of the reovirus particles after onset of lateral motion ($T_3 + T_4$) as a function of t. This period includes the time elapsed immediately preceding clathrin uncoating.

tive view of the dynamics of clathrin coat assembly and disassembly at the surface of BSC1 and COS cells under the growth conditions described. We have also followed specific cargo capture in a subset of the clathrin clusters to ensure that the overall analysis applies to genuine endocytic vesicles and to identify the fate of vesicles after loss of clathrin.

We derive from our data the following description of

clathrin dynamics. A large fraction of coated pits nucleates at randomly distributed points within permissive areas of the cell surface. In BSC1 cells (stably expressing tagged LCa or σ2 or transiently expressing tagged LCa), there is little correlation between positions at which coated pits assemble and the positions from which previous pits have budded. The situation is different in COS cells, which show a subset of coats assembling at preferred regions, as previously described (Gaidarov et al., 1999). We believe that the available evidence does not support a model in which the plasma membrane contains specialized sites acting as factories to sustain the continuous assembly of many coated pits. We propose instead that recruitment of coat components occurs randomly within a large number of active domains scattered throughout the plasma membrane and surrounded by regions of low activity, presumably constrained by the underlying cytoskeleton.

The duration of the nucleation step cannot be determined from current data, because this step probably involves too few clathrin triskelions and AP-2 complexes to detect. Once an assembly has become visible, however, it grows at a steady rate, and the extrapolation from the insets in Figure 2B and 2E suggests that, in our experiments, a newly visible pit might be 10–20 seconds old. Dynamin and AP-2 appear in assembling pits along with clathrin, and the strengths of these fluorescent signals grow in parallel.

The rate of clathrin assembly can be estimated from the likely size of a coated vesicle with a total visible lifetime of 32 s, the peak of the distribution in Figure 2B. Our size-intensity calibration (Figure 2C) predicts that a 32 s vesicle corresponds to the abundant soccer ball structure (90–100 nm outer diameter) with 60 triskelions (Musacchio et al., 1999). Because the clathrin signal continues to increase throughout the measurable lifetime of the cluster, we calculate from the data in Figure 5 that the rate of growth is between one and two clathrin triskelions per second. The 6-second-old pits that capture transferrin will have 10–20 clathrins—just enough to form a slightly curved indentation in the plasma membrane but not enough to close in around even the smallest cargo; the 20-second-old pits that capture LDL will have ~40 clathrins and will be more indented before acquiring the remaining 40–120 clathrins needed to make a larger coat. AP-2 recruitment parallels clathrin assembly. Our experiments do not have sufficient resolution to determine whether the first clathrin precedes or follows an AP complex, nor can we be certain at the 1 s level whether clathrin uncoating precedes or follows AP dissociation. But the simplest interpretation of our data is that AP association and dissociation depend simply on what is happening to the clathrin scaffold. This interpretation differs from one based on TIRF microscopy of cells transiently expressing LCa-dsRED and EGFP-α-adaptin (Rappoport et al., 2003). The authors of that study reported that the α chain signal appeared in stable patches of LCa-dsRED but was absent in the "blinking" LCa-dsRED clusters. Our observations demonstrate clearly that authentic coated vesicles, active in endocytosis of transferrin, LDL, or reovirus, have short (35–400 s) lifetimes and contain adaptors. The association of AP-2 with coated pits and vesicles is also, of course, consistent with their biochemical copurification.

Short-Lived Pits May Be Abortive

The most unexpected result of our analysis is the detection of a large number of relatively dim, very short-lived clathrin clusters. What is the significance of these events? It is possible that these short-lived clusters represent a subset of more rapidly growing coats that mature and pinch off quickly. Their weak fluorescence intensity argues against this interpretation, however. Their brightness corresponds to their age, calibrated as described, and we estimate that they contain not more than 30 triskelions. Moreover, their disappearance is generally not accompanied by the burst of dynamin intensity seen just before budding of the larger structures, nor is it preceded by the rapid positional shift that signals pinching off. We therefore believe that a likely interpretation of the short-lived clusters is that they are abortive coated pits. Partially formed pits, in equilibrium between addition and loss of clathrin, might be expected on occasion to disassemble completely, especially if they contained less than 20–30 triskelions. A specific event, perhaps linked to capture of cargo, might stabilize the nascent coated pit and thus commit it to finish assembly and to bud. Indeed, the average lifetime of the short-lived clusters is less than the age at the time of uncoating of a coated vesicle loaded with cargo. We suggest that the coated pits that continue to completion of an endocytic event are generally those loaded with cargo of some kind, of which the transferrin in our experiments will have labeled a larger proportion than the LDL and reovirus.

Cargo Capture and Commitment to Completion

The model just attained makes predictions that we can test with our data. One of these is that, once cargo and clathrin are together, clathrin assembly should proceed to coated vesicle budding and uncoating. Indeed, in the fields we analyzed, no transferrin- or LDL-associated coated pits and very few reovirus-associated coated pits failed to proceed to completion.

A second prediction of our model concerns the likelihood of detecting clathrin associated with a reovirus particle when compared with the likelihood of detecting clathrin at a random position on the cell membrane. We scored fields in the reovirus time series for the number of clathrin clusters per unit area and for the fraction of virus particles associated with clathrin (Supplemental Table S1). We assumed a random distribution of nucleation events (see Figure 3) and calculate the likelihood of clathrin appearing within an area equal to the "footprint" of a virus particle (between 0.03 and 0.1 μ^2, depending on assumptions of the calculation, see Supplemental Table S1) and within a time equal to the mean lifetime of a coated pit (40 s). If association of cargo with a coated pit simply increases its lifetime by committing it to finish the assembly of a clathrin lattice of suitable size, then the likelihood of finding clathrin associated with a reovirus particle should be the likelihood above, multiplied by the proportional increase in lifetime of the coated pit (400/40). The calculated likelihood is between 0.05 and 0.17, in good agreement with the observed value of 0.13 ± 0.02 (Supplemental Table S1). We conclude from this calculation that there is no evidence that the reovirus-receptor complex directly induces coated

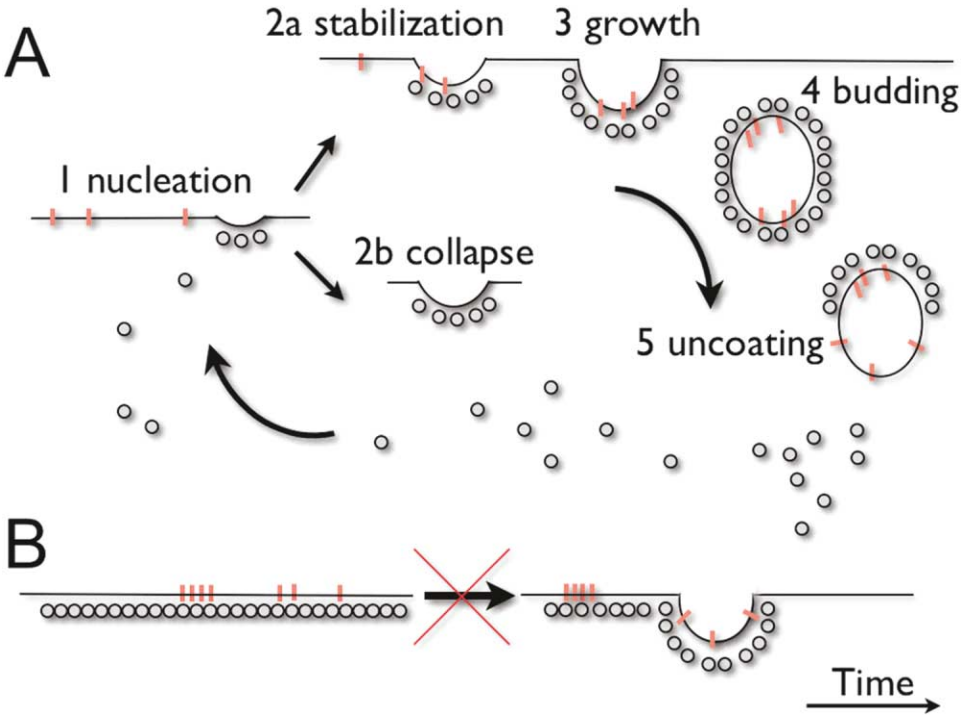

Figure 8. Model for the Life of an Endocytic Clathrin-Coated Pit

(A) The principal molecular stages (1–8) in our proposed exploratory model for coated pit and vesicle formation. The gray line represents the plasma membrane; gray circles, clathrin and adaptors and other coat proteins; orange lines, membrane bound cargo. (1) Nucleation of coat assembly by recruitment of as yet unidentified components to randomly distributed positions on the inner surface of the plasma membrane. (2) During an initial exploratory phase, coated pits continue to grow but (3) collapse rapidly if conditions required for coat stabilization are not met. (4) Alternatively, the forming coated pit stabilizes, perhaps by cargo capture. (5) Continued growth accompanied by further invagination of the membrane. (6) Membrane constriction and neck formation, followed by (7) a final burst of dynamin recruitment and fission of the connecting membranous neck. After budding, the coated vesicle moves away from the membrane. (8) Uncoating ensues within a few seconds of budding. This model is consistent with the on-off behavior and growth characteristics of the coat.

(B) Alternative model for coated pit and vesicle formation. Cargo is captured by clathrin and other coat components that have first assembled as a large and relatively stable flat array. The deeply invaginated coated pits form either by complete reorganization of the flat array or by partial reorganization and release of a small patch of coat.

pit formation, even though the apparent likelihood of finding clathrin associated with virus is higher than for a similar but randomly selected area of membrane. Rather, the presence of virus determines that the lifetime of a pit that happens to form beneath it will be substantially longer than average (Supplemental Figure S1). Simulation of the association of LDL and clathrin has led us to the same conclusion (Supplemental Figure S1).We asked what would be the mean time to capture for a particle diffusing toward a target in two dimensions, assuming a footprint of 15 nm for the interacting parts of the LDL receptor and the clathrin coat. The simulated values range between 17 and 28 s, in excellent agreement with the observed one (20 s). Thus, as with reovirus, LDL/LDL receptor complexes do not seem to induce coated pit formation; instead, they are captured by an already partially assembled coated pit.

Dynamin

We observed steady recruitment of dynamin followed in some cases by a burst of additional dynamin association, in agreement with previous real-time studies of the colocalization of dynamin1-EGFP and clathrin on cell surfaces (Merrifield et al., 2002). Although the analysis in this earlier work was restricted to the interval just prior to clathrin uncoating, it clearly showed the presence of dynamin1 in clathrin clusters before the final burst. More recent studies following a relatively small number of pits and likewise restricted to the interval just prior to uncoating also show dynamin2 in assembling clathrin clusters, although they do not show a detectable final burst of intensity (Rappoport and Simon, 2003). These data and ours help to resolve the long-standing puzzle presented by the presence of dynamin embedded within the clathrin lattice as detected by immunoelectron microscopy (Damke et al., 1994). The short duration of the dynamin burst and the rapidity with which uncoating ensues probably explain why rings of accumulated dynamin have not been seen at the neck of budding vesicles in thin-section electron micrographs.

There is no evidence that dynamin interacts directly with clathrin or its adaptors, but it does bind through its C-terminal, proline-rich segment to a number of different SH3-domain containing proteins, such as amphiphysin, which in turn can interact with clathrin and its adaptor AP-2 (David et al., 1996). Dynamin also appears to interact with Hsc70 and auxilin, both of which associate with clathrin (Newmyer et al., 2003). It is possible that, in

addition to having a role in fission, dynamin participates in some other way in regulating assembly of a clathrin coat. It might, for example, act as a molecular antenna, to recruit lipid-modifying enzymes such as endophilin (Farsad et al., 2001), which could help to deform the membrane lying under the clathrin lattice.

Model

We summarize our conclusions with a tentative molecular description of the life of an endocytic, clathrin-coated pit (Figure 8). Assembly nucleates by recruitment of as yet unidentified components to randomly distributed positions on the inner surface of the plasma membrane. Addition of clathrin proceeds at a steady rate (in these cells) of about one triskelion every 2 s. Dynamin and AP-2 are added to the coated pit along with clathrin (and presumably other components that we have not yet labeled). Assembly aborts unless a molecular event, perhaps linked to cargo loading, commits the coated pit to completion and budding. Cargo recruitment, at least in the case of laterally mobile cargo such as transferrin or LDL receptor bound, occurs when the pit contains about 10–40 triskelions, which is also the stage at which abortive assembly terminates. The dissolution of abortive assemblies is rapid, and whether it is an active process (catalyzed, for example, by Hsc70) or results simply from the failure of some molecular clamp to fix the nascent structure is an important open question. The critical point appears to occur just when membrane curvature might begin to resist further growth of the clathrin lattice. The size of the coated vesicle, and hence the design of its clathrin lattice and the time it takes to achieve its final form, is determined by the size of the cargo. Pinching off, detected by sudden movement of the clathrin cluster, is followed within about 10 s by rapid loss of clathrin and AP-2. The newly uncoated vesicle then undergoes a directed motion away from the budding point, presumably along a cytoskeletal track. Extension of our experimental design to include other components of an assembling coated pit will enable us to describe the sequence and rates of many of the molecular events about which, at present, we can only speculate.

Our observations suggest that the clathrin-based endocytic machinery has an exploratory character, rather like the microtubule cytoskeleton. Microtubules nucleate at an organizing center, grow steadily, and collapse "catastrophically" unless their growing end is captured by a suitable target (Mitchison and Kirschner, 1984). Likewise, the coated pits we have followed appear to dissolve abruptly unless some intervening event determines that they continue. One event that clearly correlates with such commitment is cargo loading, and we suggest that the molecular mechanism by which a pit is stabilized and its growth allowed to proceed is linked to the structures that carry out receptor sorting. For example, interaction of AP-2 with peptides containing tyrosine-based endocytic sorting signals increases substantially when AP-2 becomes part of a clathrin coat (Rapoport et al., 1997). Conversely, cargo recognition must enhance AP-2 affinity for clathrin. One or more such interactions could create a commitment signal. A molecular basis for the rapid disassembly of an "uncommitted" coated pit might be found in the dynamics of Hsc70 recruitment, the properties of GTPases involved in adaptor association, or in other activities not yet described.

The model just outlined separates the mechanism of initiation from the process of cargo recognition. It allows a variety of different cargo adaptors to participate equally, rather than making one a privileged initiator, and it avoids the need to postulate differentiated budding sites on the membrane. Critical tests of this description of endocytosis as an exploratory process will be finding the mechanism by which abortive coated pits collapse and defining the signaling process that allows assembly to proceed.

Experimental Procedures

Preparation of Plasmid, Virus, and Expresser Cells

LCa-YFP and LCa-mRFP were made by fusing DNA (amplified by PCR) encoding rat brain clathrin light chain, LCa1 (Kirchhausen et al., 1987), to the 3′ end of the coding sequence for EYFP (Clontech) or mRFP. Reovirus type I Lang was purified from infected L929 cells. Productive infection was determined by a single-cell-based immunofluorescence assay (DeTulleo and Kirchhausen, 1998) that detected the newly synthesized nonstructural protein μNS. BSC1 monkey kidney epithelial cells stably expressing LCa-YFP were obtained by transfection and maintained by selection with G418 in DMEM supplemented with 10% fetal bovine serum. Simultaneous transient expression of LCa-mRFP and dynamin2-EGFP was obtained in monkey COS cells by DEAE Dextran-aided transfection of a mixture of plasmids at molar ratio of 2:1. Under these conditions, expression of the constructs had no discernable effects on cell shape or growth.

Preparation of Cells for Imaging

BSC1 cells stably expressing LCa-YFP were imaged 18–40 hr after plating on 25 mm diameter glass cover slips at a density of 20,000–40,000 cells per well. When needed, transient expression of Δ95–295Eps15 and dynamin^{K44A} was achieved by transfection of the cells 24 hr after plating and the cells imaged 48–72 hr later. COS cells (20,000–40,000) were plated on 25 mm diameter glass cover slips and imaged 14 hr after transfection with LCa-mRFP and dynamin2-EGFP. For imaging, the cells were transferred to α-MEM supplemented with 20 mM HEPES (pH 7.2) and 0.5% bovine serum albumin in the absence of phenol red.

Imaging

Images were acquired with a spinning disk confocal head (Perkin Elmer Co., Boston, MA) coupled to a fully motorized epifluorescence microscope (Axiovert 200M; Carl Zeiss, Inc.; Thornwood, NY) using 63× or 100× lenses (Carl Zeiss, Inc) under control of SlideBook 4 (Intelligent Imaging Innovations, Denver, CO). Digital images (12 bit) were obtained with a cool CCD camera (Cool Snap HQ, Photometrics, Trenton, NJ) with 2 × 2 binning and spatial resolution of 130 or 200 nm/pixel for the 100× and 63× lenses, respectively. Images were acquired with exposure times between 800 and 1200 milliseconds from cells maintained at 37°C using a heated stage (20/20 Technology, Inc.; Wilmington, NC). A krypton-argon laser (Mellets Griot, Carlsbad, CA) emitting at 488, 568, and 647 nm was used to excite YFP, EGFP, mRFP, 1,1′-dioctadecyl-3,3,3′,3′-tetramethylindocarbocyanine perchlorate (DiI)., Alexa568, Alexa594, and Alexa647.

Image Processing

The following sequential steps were used to identify and track clathrin and dynamin clusters. (1) Creating a mask. We applied a 2D deconvolution to each raw image to increase signal-to-noise ratio and to even out background. We smoothed the deconvolved images by applying a Gaussian 2D radial transformation (radius, one pixel) and identified fast spatial changes by applying a Laplacian 2D derivative. Finally, a mask corresponding to each spot in the

images was obtained by AND logical operation applied between the images resulting from the Laplacian transformation and the deconvolved images segmented by intensity. (2) Spot identification. We determined the spatial coordinates for the centroids of every masked spot in any given image. Spots larger than three pixels in radius (100 × lens) were eliminated from further analysis, as they would be larger than the diffraction-limited images of the 100–200 nm diameter coated pits we wished to follow. (3) Spot tracking. We connected the masked spots in time by allowing the software to explore the position of every spot along the time series, removing objects moving two or more pixels in the x-y plane, e.g., a radius of $(2)^{1/2}$ between time frames. Only spots that satisfied this spatial constraint for three or more consecutive time frames were accepted. We define the net fluorescence intensity of each spot masked in the raw image as the difference in fluorescence intensity within the mask minus the average background signal of the cytosol.

Fluorescence Intensity Calibration

We used clathrin-coated vesicles isolated from the BSC1 cells stably expressing Lca-EGFP to relate the net fluorescence intensity measured from coated pits in these cells to the number of clathrin triskelions they contain. The size and type of clathrin-coated structures present in the preparation was determined by electron microscopy of samples negatively stained with 1.2% uranyl acetate (Gallusser and Kirchhausen, 1993). Clathrin-coated vesicles were purified by high-speed centrifugation in the presence of 100 mM MES (pH 6.5) (Clairmont et al., 1997), transferred to a solution of pH 7.0 (to avoid the pH-dependent fluorescent quenching of EGFP), and imaged under the same acquisition conditions used for imaging living cells. Brief (15 min) chemical crosslinking (1 μg protein/0.01 μg DSP) (Kirchhausen and Harrison, 1981) was used to prevent spontaneous uncoating of the vesicles due to adsorption onto the surface of the glass cover slip.

Acknowledgments

We thank Dr. M. Krieger, M. Penman, S. Xu, and Y. Zhu for providing human DiI-LDL; Dr. McNiven and Dr. R. Tsien for providing the constructs for human dynamin2-EGFP and monomeric RFP; Dr. J. Parker for help and advice on the isolation of reovirus; Drs. V. Chandru and J. Guanawardena for help in the early stages of image processing; Dr. R. Massol for help and advice on many aspects of image acquisition; and Dr. C. Monks and M. Roden for developing key features in SlideBook 4. We thank Dr. S.C. Harrison for extensive and fruitful discussions. M.E. is a Dorot Fellow and acknowledges support from the Fulbright Foundation. We thank the Perkin Foundation for making available funds to help in purchasing the imaging equipment. Supported by NIH GM36548 (T.K).

Received: January 12, 2004
Revised: July 9, 2004
Accepted: July 15, 2004
Published: September 2, 2004

References

Bonifacino, J.S., and Traub, L.M. (2003). Signals for sorting of transmembrane proteins to endosomes and lysosomes. Annu. Rev. Biochem. *72*, 395–447. Published online March 6, 2003. 10.1146/annurev.biochem.72.121801.161800.

Brodsky, F.M., Chen, C.Y., Knuehl, C., Towler, M.C., and Wakeham, D.E. (2001). Biological basket weaving: formation and function of clathrin-coated vesicles. Annu. Rev. Cell Dev. Biol. *17*, 517–568.

Clairmont, K.B., Boll, W., Ericsson, M., and Kirchhausen, T. (1997). A role for the hinge/ear domain of the beta chains in the incorporation of AP complexes into clathrin-coated pits and coated vesicles. Cell. Mol. Life Sci. *53*, 611–619.

Conner, S.D., and Schmid, S.L. (2003). Regulated portals of entry into the cell. Nature *422*, 37–44.

Damke, H., Baba, T., Warnock, D.E., and Schmid, S.L. (1994). Induction of mutant dynamin specifically blocks endocytic coated vesicle formation. J. Cell Biol. *127*, 915–934.

David, C., McPherson, P.S., Mundigl, O., and De Camilli, P. (1996). A role of amphiphysin in synaptic vesicle endocytosis suggested by its binding to dynamin in nerve terminals. Proc. Natl. Acad. Sci. USA *93*, 331–335.

DeTulleo, L., and Kirchhausen, T. (1998). The clathrin endocytic pathway in viral infection. EMBO J. *17*, 4585–4593.

Farsad, K., Ringstad, N., Takei, K., Floyd, S.R., Rose, K., and De Camilli, P. (2001). Generation of high curvature membranes mediated by direct endophilin bilayer interactions. J. Cell Biol. *155*, 193–200.

Forrest, J.C., Campbell, J.A., Schelling, P., Stehle, T., and Dermody, T.S. (2003). Structure-function analysis of reovirus binding to junctional adhesion molecule 1. Implications for the mechanism of reovirus attachment. J. Biol. Chem. *28*, 48434–48444. Published online September 9, 2003. 10.1074/jbc.M305649200.

Fujiwara, T., Ritchie, K., Murakoshi, H., Jacobson, K., and Kusumi, A. (2002). Phospholipids undergo hop diffusion in compartmentalized cell membrane. J. Cell Biol. *157*, 1071–1081.

Gaidarov, I., Santini, F., Warren, R.A., and Keen, J.H. (1999). Spatial control of coated-pit dynamics in living cells. Nat. Cell Biol. *1*, 1–7.

Gallusser, A., and Kirchhausen, T. (1993). The β1 and β2 subunits of the AP complexes are the clathrin coat assembly components. EMBO J. *12*, 5237–5244.

Goldstein, B., Wofsy, C., and Bell, G. (1981). Interactions of low density lipoprotein receptors with coated pits on human fibroblasts: estimate of the forward rate constant and comparison with the diffusion limit. Proc. Natl. Acad. Sci. USA *78*, 5695–5698.

Hansen, S.H., Sandvig, K., and van Deurs, B. (1992). Internalization efficiency of the transferrin receptor. Exp. Cell Res. *199*, 19–28.

Heuser, J. (1989). Effects of cytoplasmic acidification on clathrin lattice morphology. J. Cell Biol. *108*, 401–411.

Kirchhausen, T. (1999). Adaptors for clathrin mediated traffic. Annu. Rev. Cell Dev. Biol. *15*, 705–732.

Kirchhausen, T. (2000). Clathrin. Annu. Rev. Biochem. *69*, 699–727.

Kirchhausen, T., and Harrison, S.C. (1981). Protein organization in clathrin trimers. Cell *23*, 755–761.

Kirchhausen, T., Scarmato, P., Harrison, S.C., Monroe, J.J., Chow, E.P., Mattaliano, R.J., Ramachandran, K.L., Smart, J.E., Ahn, A.H., and Brosius, J. (1987). Clathrin light chains LCA and LCB are similar, polymorphic and share repeated heptad motifs. Science *236*, 320–324.

Merrifield, C.J., Feldman, M.E., Wan, L., and Almers, W. (2002). Imaging actin and dynamin recruitment during invagination of single clathrin-coated pits. Nat. Cell Biol. *4*, 691–698.

Merrifield, C.J., Qualmann, B., Kessels, M.M., and Almers, W. (2004). Neural Wiskott Aldrich Syndrome Protein (N-WASP) and the Arp2/3 complex are recruited to sites of clathrin-mediated endocytosis in cultured fibroblasts. Eur. J. Cell Biol. *83*, 13–18.

Mitchison, T., and Kirschner, M. (1984). Dynamic instability of microtubule growth. Nature *312*, 237–242.

Musacchio, A., Smith, C.J., Roseman, A.M., Harrison, S.C., Kirchhausen, T., and Pearse, B.M.F. (1999). Functional organization of clathrin in coats: combining electron cryomicroscopy and X-ray crystallography. Mol. Cell *3*, 761–770.

Newmyer, S.L., Christensen, A., and Sever, S. (2003). Auxilin-dynamin interactions link the uncoating ATPase chaperone machinery with vesicle formation. Dev. Cell *4*, 929–940.

Orth, J.D., and McNiven, M.A. (2003). Dynamin at the actin-membrane interface. Curr. Opin. Cell Biol. *15*, 31–39.

Paul, R.W., Choi, A.H., and Lee, P.W. (1989). The alpha-anomeric form of sialic acid is the minimal receptor determinant recognized by reovirus. Virology *172*, 382–385.

Rappoport, J.Z., and Simon, S.M. (2003). Real-time analysis of clathrin-mediated endocytosis during cell migration. J. Cell Sci. *116*, 847–855.

Rapoport, I., Miyazaki, M., Boll, W., Duckworth, B., Cantley, L.C., Shoelson, S., and Kirchhausen, T. (1997). Regulatory interactions in

the recognition of endocytic sorting signals by AP-2 complexes. EMBO J. *16*, 2240–2250.

Rappoport, J.Z., Taha, B.W., Lemeer, S., Benmerah, A., and Simon, S.M. (2003). The AP-2 complex is excluded from the dynamic population of plasma membrane-associated clathrin. J. Biol. Chem. *278*, 47357–47360.

Reynolds, G.D., and St. Clair, R.W. (1985). A comparative microscopic and biochemical study of the uptake of fluorescent and 125I-labeled lipoproteins by skin fibroblasts, smooth muscle cells, and peritoneal macrophages in culture. Am. J. Pathol. *121*, 200–211.

Ripley, B.D. (1976). The second-order analysis of stationary point processes. J. Appl. Probab. *13*, 255–266.

Sako, Y., and Kusumi, A. (1994). Compartmentalized structure of the plasma membrane for receptor movements as revealed by a nanometer-level motion analysis. J. Cell Biol. *125*, 1251–1264.

REQUIRED VIEWING: SUPPLEMENTAL MOVIES:
http://download.cell.com/supplementarydata/cell/118/5/591/DC1/index.htm
Supplemental Data for:

Ehrlich et al., Cell *118*, pp. 591–605

Document S1 Sampling Statistics
Supplemental Figure S1.

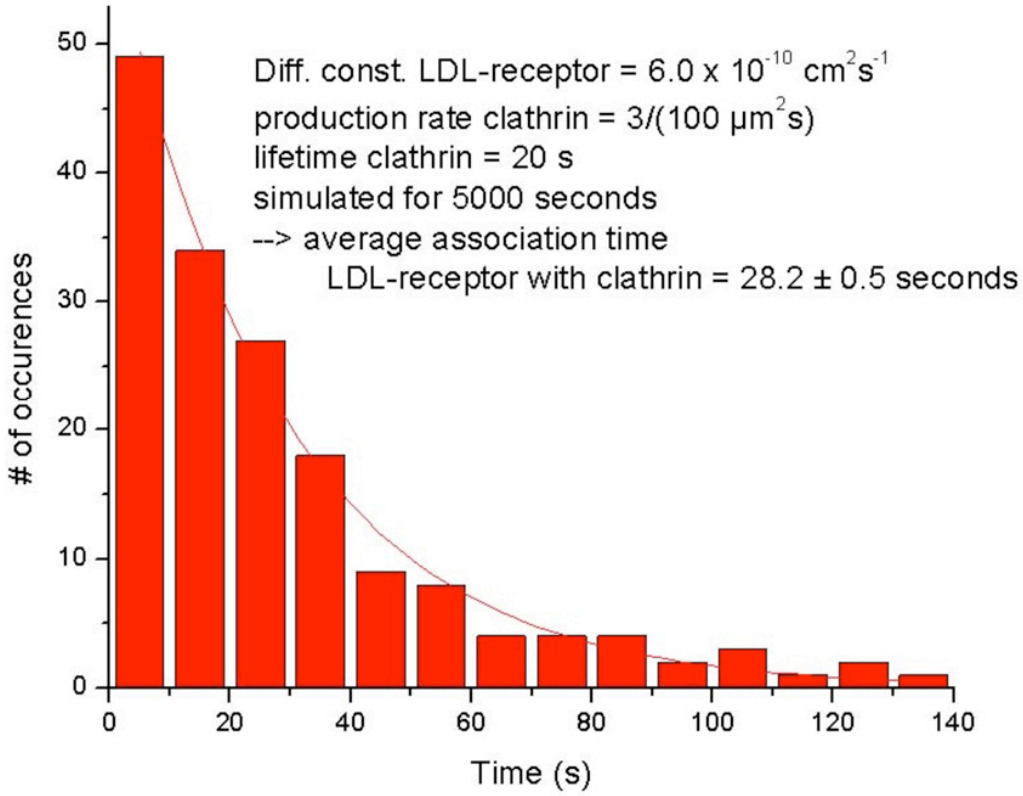

Calculation of Association Times between LDL and a Forming Clathrin-Coated Pit
To substantiate the experimental times measured for the association of a coated pit with an LDL/LDL receptor complex, we estimated this time by computational and analytical means. MATLAB (Mathworks, Natick, MA) was used to simulate a two-dimensional random of a particle (the LDL/LDL receptor complex) on a grid with a size of 50 ´ 50 μm^2. This field also contained randomly appearing clathrin pits, whose creation and lifetime dynamics matched the experimental observations (three events per 10^8 nm^2 per second, lifetime 20 s). The step size of the simulation assumes a footprint of 15 nm for the interacting parts of the LDL receptor and the clathrin coat. Combined with a stepping time of 1 ms, this results in a two-dimensional diffusion constant for the LDL receptor of 6 ´ 10-10 cm^2/s. Simulations were performed for 5000 steps (5 s), and association times of LDL/LDL receptor complexes by a coated pit with were recorded and displayed as an histogram. The distribution can be accurately fit with a monoexponential decay with a time constant of 28 □ 1 s. An analytical expression for the mean diffusion time t in two dimensions required to reach a small target of radius a in the middle of a space of radius R ($R >> a$) is given by

where D indicates the two-dimensional diffusion constant (Creighton, 1993). The radius R describes the area in which we can find exactly one clathrin pit with which the LDL/LDL receptor complex can associate. Given the experimental observation that three pits are created per 10^8 nm^2 per s and a pit lifetime of 20 s, R equals 730 nm. For a = 15 nm and D = 6 ´ 10-10 cm^2/s, this results in an association time of 17.2 s.
Supplemental Movie S1. Dynamic Behavior of Clathrin-Coated Pits and Vesicles Labeled with LCa-YFP
Time-lapse series (120 frames, 10 s intervals acquired at 37°C) obtained from a cell constitutively expressing LCa-YFP using the spinning disk confocal microscope.

Supplemental Movie S2. Dynamic Behavior of Clathrin-Coated Pits and Vesicles Labeled with s2-EGFP
Time-lapse series (200 frames, 3 s intervals acquired at 37°C) obtained from a cell constitutively expressing s2-EGFP using the spinning disk confocal microscope.

Supplemental Movie S3. Automatic Selection of Clathrin Clusters Labeled with LCa-YFP by Spot Determination and Particle Tracking
The time-lapse series (100 frames, 3 s intervals acquired at 37°C and subjected to no neighbor deconvolution) corresponds to a confocal optical section obtained from the bottom surface of a BSC1 cell constitutively expressing LCa-YFP (green) and includes the position and shape of the overlapping masks as determined by the automated procedure implemented in SlideBook 4 (blue).

Supplemental Movie S4. Automatic Selection of Clathrin Clusters Labeled with s2-EGFP by Spot Determination and Particle Tracking
The time-lapse series (200 frames, 3 s intervals acquired at 37°C) corresponds to a confocal optical section obtained from the bottom surface of a BSC1 cell constitutively expressing s2-EGFP (green) and includes the position and shape of the overlapping masks as determined by the automated procedure implemented in SlideBook 4 (blue).

Supplemental Movie S5. Inhibition of DiI-LDL Entry by Transient Treatment of the Cells with Hypertonic Sucrose
The time-lapse series (60 frames, 10 s intervals acquired at 37°C) corresponds to a confocal optical section obtained from the top surface of a BSC1 cell constitutively expressing LCa-YFP (green) pretreated for 30 min with hypertonic media (media supplemented with 0.45 M sucrose). DiI-LDL (red) was added 5 min prior to image acquisition. This treatment prevents the dynamic behavior of clathrin and blocks the accumulation of DiI-LDL inside cells. Under this condition, the motion of DiI-LDL on the cell surface is not affected.

Supplemental Movie S6. Cholesterol Depletion Interferes with the Dynamics of Clathrin-Coated Pits and Vesicles
The time-lapse series (60 frames, 10 s intervals acquired at 37°C) corresponds to a confocal optical section obtained from the bottom surface of a BSC1 cell constitutively expressing LCa-YFP (green) pretreated with ~10 M b-methyl cyclodextrin for 30 min. Transferrin alexa647 was added for another 20 min before acquisition of the movie. The first frame shows absence of the fluorescent signal of transferrin alexa647 (blue) inside cells and its accumulation in the cell surface, consistent with a complete block of its receptor-mediated endocytosis mediated by the clathrin pathway. The LCa-YFP signals (green) are mostly static.

Supplemental Movie S7. Expression of Dynamin 2K44A Interferes with the Dynamics of Clathrin-Coated Pits and Vesicles
The time-lapse series (60 frames, 10 s intervals acquired at 37°C) corresponds to a confocal optical section obtained from the bottom surface of a BSC1 cell constitutively expressing LCa-YFP (green) and transiently expressing dynamin 2 ^{K44A}-RFP for 80 hr (red). Transferrin Alexa647 (blue) was added for 20 min before acquisition of the movie. The first frame shows absence of the fluorescent signal of transferrin alexa647 (blue) inside cells and its accumulation in the cell surface, consistent with block of its receptor-mediated endocytosis.

Supplemental Movie S8. Dynamic Behavior of Clathrin and Dynamin
The time-lapse series (30 frames, 6 s intervals acquired at 37°C) corresponds to a confocal optical section obtained from the bottom surface of a COS cell transiently expressing LCa-mRFP (red) and dynamin2-EGFP (green). The outlines illustrate examples of short- and long-lived pits. The long-lived pit displays the characteristic increase in the dynamin signal, followed by the lateral movement of the clathrin vesicle and ending with uncoating.

Supplemental Movie S9. Capture of a Single LDL Particle by a Clathrin-Coated Pit and its Internalization by a Coated Vesicle
Time-lapse series (149 frames obtained with 2.6 s intervals and imaged at 37°C) from a BSC1 cell expressing LCa-YFP (green) and incubated with fluorescently labeled DiI-LDL (red). This example shows the migration and capture of an LDL particle to a newly formed coated pit followed by their coassociation and ending with clathrin uncoating and movement of the LDL particle inside the cell.

Supplemental Movie S10. Capture of a Single Reovirus Particle by a Clathrin-Coated Pit and its Internalization by a Coated Vesicle

Time-lapse series (two consecutive acquisitions of 50 frames obtained with 4 s intervals and imaged at 37°C) from a BSC1 cell expressing LCa-YFP (green) and incubated with Alexa647-labeled reovirus (red). This example shows assembly of a newly formed coated pit under a stationary reovirus particle, followed by acquisition of lateral motion of the virus/clathrin coat complex and ending with clathrin uncoating and further movement of the virus inside the cell. Scale bar, 1 mm.

Supplemental Movie S11. Inhibition of Reovirus Entry by Transient Treatment with Hypertonic Sucrose Time-lapse series (50 frames, 20 s intervals acquired at 37°C) corresponds to a confocal optical section from the top surface of a BSC1 cell constitutively expressing LCa-YFP (green) pretreated for 30 min with hypertonic media (media supplemented with 0.45 M sucrose). Alexa647 reovirus (red) was added for 20 min prior to acquisition of the movie. Incubation with hypertonic media prevents the dynamic behavior of clathrin and blocks virus uptake (represented here by absence of mobile virus). The highly mobile reovirus particles are those free in the bathing medium. We also used the same blocking conditions but only applied during the infection period carried out using a multiplicity of infection of 0.2–0.5; based on a single cell immunofluorescence-based assay (DeTulleo and Kirchhausen, 1998), we observed a substantial decrease in reovirus infection (reduction of 84%, n = 288).

Supplemental Movie S12. Inhibition of Reovirus Entry by Transient Expression of D95–295 Eps15-EGFP Time-lapse series (20 frames, 10 s intervals acquired at 37°C) corresponds to a confocal optical section of two adjacent cells, the one in the left transiently expressing D95–295 Eps15-EGFP (green). Alexa647 reovirus (red) was added for 75 min prior to acquisition of the movie. Most reovirus particles are immobile and remain on the plasma membrane in the cell (left) expressing D95–295 Eps15-EGFP. Reovirus internalizes and becomes mobile inside the nonexpressor cell used as a control (right). Using the single cell immunofluorescence-based assay and a multiplicity of infection of 0.2–0.5, we observed a reduction of almost 50% in the frequency of reovirus infection in cells blocked in their clathrin-mediated transferrin uptake by expression of D95–295Eps15 (n = 192).

Supplemental Table S1.

Supplemental Table S1.

Fraction of reovirus particles associated with a coated pit[a]	0.13 ± 0.02
Coated pit/μ^2 of cell membrane (counted in three fields, with areas in the range between 600 and 1200 μ^2)[b]	0.17 ± 0.03
Mean coated lifetime[c]	43 s
Mean lifetime of a reovirus associated with a coated pit[d]	400 s
Footprint of reovirus[e]	
Estimate 1 (by surface area)	0.03 μ^2
Estimate 2 (by area visited in 20 s by diffusion assuming D ~ 10^{-11} cm^2/s)	0.01 μ^2

[a]Determined by counting a total of 531 virus particles in three randomly chosen fields.

[b]Determined by counting all coated pits in the three fields selected for [a].

[c]See Figures 2B and 3A.

[d]See Figure 6B.

[e]D ~ 10^{-11} cm^2/s is approximately 1/50 the mean LDL diffusion constant (Figure 5C), estimated by taking the ratio of the diameter within the membrane of LDL bound receptors (two transmembrane helices, ~ 2 nm) to the 100 nm diameter of the reovirus (presumed to have multiple membrane attachments with a maximum separation equal to its diameter).

Supplemental Data for:

Ehrlich et al., Cell *118*, pp. 591–605

Sampling Statistics

As background fluctuations of fluorescence intensity have an inherent random distribution that could bias our results, it was critical to rule out the possibility of incorrect identification of weak fluorescent signals. This was done by examining the noise level within the tracked data following the analysis of sampling statistics in the images. We determined the standard deviation of the background fluorescence (13.5 ± 0.5 fluorescent units) and then looked for the weakest spots assigned as coated pits. Their peak intensity (16 fluorescence units after background subtraction) results in a signal-to-noise ratio of 16/13.5 = 1.185. Assuming that these fluorescent clusters are Gaussian in shape (size of 3 × 3 pixels) and assuming a full-width half-maximum of 3 pixels, the average fluorescent intensity in each pixel of a cluster is roughly five sixths of that of the center pixel, or 13.33 fluorescence units, Thus, the average signal-to-noise for all pixels within the cluster becomes 13.33/13.5 = 0.988, and, considering a standard normal distribution, the signal-to-noise ratio for a single pixel gives a significance level of 0.322, equivalent to a 67.8% chance that the signal is real. Because the fluorescent cluster contains nine such pixels, the signal-to-noise ratio improves to 2.994 with a significance level of 0.0028 (or 99.72% chance that this signal is real), since it is proportional to the square root of the sampling number. Finally, by imposing the criterion that the fluorescent spot for a coated pit has to remain in the same location in three consecutive time frames, one obtains an increase (proportional to the square root of the number of consecutive images) to 5.2 in the signal-to-noise ratio. This ratio corresponds to a significance level well below 0.0005, indicating that the weak events scored by the program (e.g., those with fluorescent intensities corresponding to 15% of the signal elicited by a complete coated vesicle) have a 99.95% likelihood of being real. Similarly, we estimate that events corresponding to 50% of the fluorescent signal elicited by a coated vesicle have a 99.9999% chance of being real.

Spatial Statistics

In spatial statistics, Ripley's K function (Ripley, 1976) is a classical tool to analyze spatial point patterns. The definition of the K function is as follows:

$$K(t) = \frac{E(d < t)}{\lambda} \qquad (1)$$

where $E(d < t)$ denotes the number of particles within a distance t of an arbitrary particle, and λ the density of particles (mean number of particles per unit area). The density can be estimated by N/A, where N is the observed number of points and A is the area of the field of view. The numerator in Equation 1 can be estimated by

$$N^{-1}\sum_{i}^{N}\sum_{j\neq i}^{N} I(d_{ij} < t) \qquad (2)$$

where d_{ij} is the distance between the ith and jth points, and $I(x)$ is the indicator function, with the value 1 if x is true and 0 if otherwise.

To prevent a bias in K(t) values at larger values of t due to the finite size of the field of view, an edge correction is introduced,

$$K(t) = \lambda^{-1}N^{-1}\sum_{i}^{N}\sum_{j\neq i}^{N} \omega(l_i, l_j) I(d_{ij} < t), \qquad (3)$$

with the weight function $\omega(l_i, l_j)$ providing the edge correction (Ripley, 1976). It has the value 1 when the circle centered at l_i and passing through the point l_j (i.e., with radius of d_{ij}) is completely inside the field of view. If part of the circle falls outside the field of view (i.e., d_{ij} is larger than the distance from l_i to at least one boundary), $\omega(l_i, l_j)$ is the proportion of the circumference of that circle that falls in the field of view.

Ripley's K function is particularly powerful to test spatial randomness, i.e., whether the spatial distribution of the events is consistent with a homogeneous Poisson process. In that case, $K(t) = \pi t^2$ for all t. To facilitate

direct comparisons to Poissonian processes, where $L(t)$ is equal to t, we use the scaled function $L(t) = (K(t)/\pi)^{1/2}$. The function $L(t)$ was calculated for every data set, consisting of the x, y positions of all observed clathrin or σ2-adaptin clusters in one particular experiment. To estimate the error for $L(t)$ of the experimental datasets, we simulated Poissonian distributions of events with identical field and sample size as the experimental data. $L(t)$ was calculated for a large number of simulations (n = 40 per dataset), and the standard deviation obtained from the distributions in $L(t)$ was adopted as an error estimate for the data presented in Figure 2. All analyses and simulations were performed in MATLAB (Mathworks, Natick, MA). The code written in MATLAB to simulate the Ripley's K function, and the diffusion of LDL is available on request.

References

Creighton, T.E. (1993). Proteins, Structures, and Molecular Properties, Second Edition. (New York: W.H. Freeman and Company).

DeTulleo, L., and Kirchhausen, T. (1998). The clathrin endocytic pathway in viral infection. EMBO J *17*, 4585–4593.

Ripley, B.D. (1976). The second-order analysis of stationary point processes. J. Appl. Probab. *13*, 255–266.